Article

Binocular visual experience drives the maturation of response variability and reliability in the visual cortex

The development of binocular response variability and reliability

Xiangwen Hao,
Qiong Liu,
Jiangping Chan,
Na Li, Xuefeng Shi,
Yu Gu

shixf_tmu@163.com (X.S.)
guyu_@fudan.edu.cn (Y.G.)

Highlights

The response reliability was driven by the mature cortical network

Integration of binocular inputs facilitated the high reliability

Normal visual experience is required for the maturation of reliability

Dark exposure can partly restore the disrupted cortical reliability
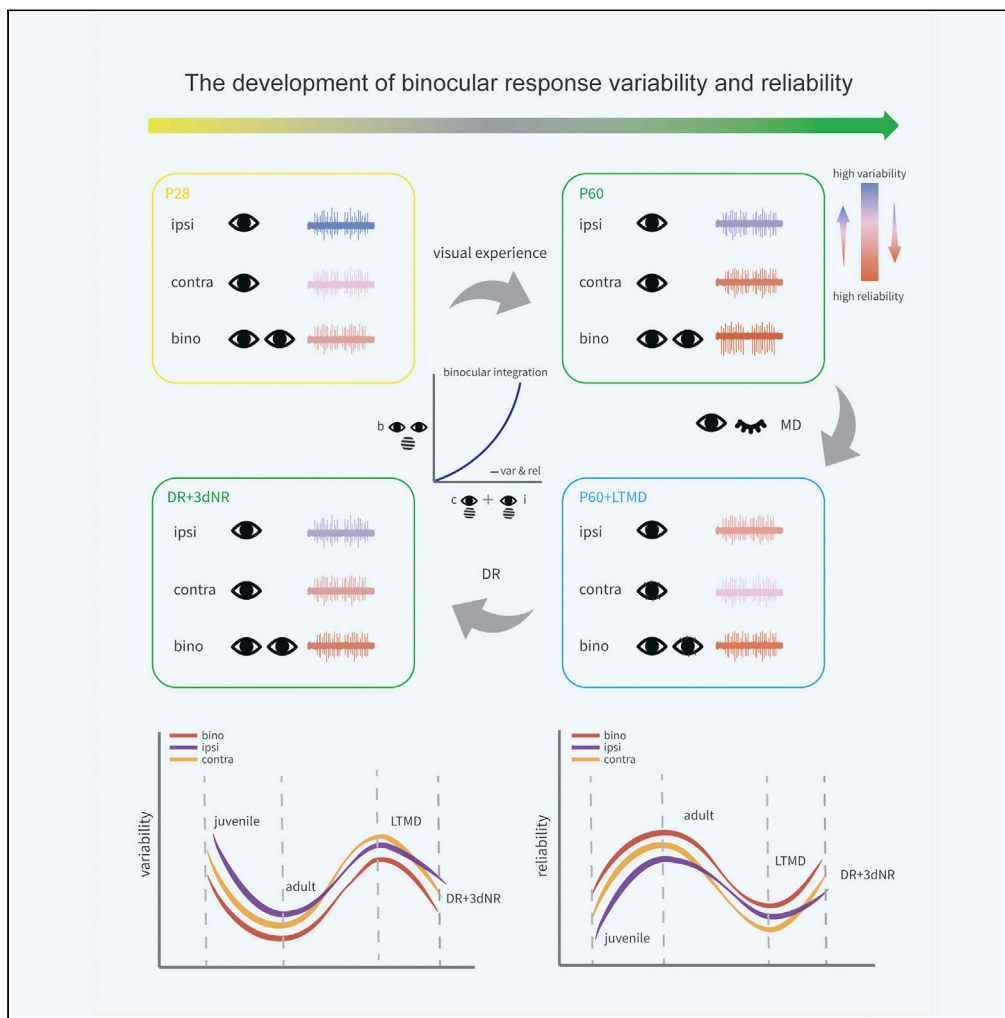
Article

Binocular visual experience drives the maturation of response variability and reliability in the visual cortex

Xiangwen Hao,[1,5] Qiong Liu,[1,2,5] Jiangping Chan,[1,5] Na Li,[1] Xuefeng Shi,[3,4,*] and Yu Gu[1,6,*]

SUMMARY

A fundamental challenge of neuroscience is to understand how a single neuron responds to multiple synaptic inputs effectively and reliably. In primary visual cortex, repeated stimuli to one eye elicit neuronal responses of inherent variability and reliability. However, it remains unclear how this monocular variability and reliability contribute to the establishment of effective and reliable binocular responses and what drives this development. In this study, using *in vivo* multichannel extracellular recordings, we demonstrate binocular responses in adult mouse visual cortex exhibit low variability and high reliability. This response characteristic is immature during the critical period of binocular vision development. In amblyopic mice, the maturation of binocular variability and reliability is disrupted, and this defect can be partially rescued by enhancing cortical plasticity via dark exposure. In conclusion, the development of cortical response variability and reliability depends on the normal binocular visual experience, which is further regulated by cortical plasticity.

INTRODUCTION

A fundamental function of a single neuron in the neural network is to effectively and reliably transmit information. The discharges of a cortical neuron often show great trial-to-trial similarity with low variance during repeated stimulation. This characteristic is crucial for reliable encoding of large amounts of sensory information in signal processing (Shadlen and Newsome, 1998). Response variability and reliability are highly related. In the primary visual cortex (V1), a high spike timing reliability reflects precise visual discrimination to the stimulation and permits information encoding with high fidelity, and a low spike count variability represents effective visual information transmission for each stimulus trial (Borst and Theunissen, 1999). However, as a neural inherent characteristic, variability can be beneficial in sensory detection for adapting to ever-changing external and internal demands (Jacobs et al., 2020; Waschke et al., 2021). Even for highly orientation-selective V1 neurons, their responses to the optimal visual stimulus could still show variances (Rossi et al., 2020). Some previous studies suggested that the variability of cortical neurons was determined by the level of spontaneous activity, as well as the animal's arousal state, environmental adaptation, and attention (Goris et al., 2014; Neske et al., 2019). However, it is recently found these factors are not the main causes for variability (de Vries et al., 2020). On the other hand, it is well established that variability originates from synaptic connections and gradually decreases along successive stages in the visual pathway (Kara et al., 2000; Faisal et al., 2008; Garrett et al., 2013). Overall, the neuronal variability and reliability might play a fundamental role in the visual information processing.

It is interesting to ask how synaptic inputs from multiple sources are integrated by a single neuron to generate effective and reliable output. Neurons in the binocular zone of V1 (V1b) receive inputs from the two eyes, whereas neurons in the monocular zone of V1 (V1m) only receive contralateral input. It is unclear whether V1b responses evoked by binocular or monocular input from either eye exhibits differences in variability and reliability. Several studies suggested that strong inputs could reduce trial-to-trial variability (Churchland et al., 2010; White et al., 2012). However, it is unknown whether the integrated binocular inputs can reduce the variability to facilitate binocular vision. It is also unknown whether the binocular integration of variability and reliability changes with development. Experience-dependent plasticity during a critical period in early life drives the development of binocular vision, such as binocular matching and disparity (Hubel and Wiesel, 1962; Vorobyov et al., 2007; Wang et al., 2010; Sarnaik et al., 2014; Scholl et al.,

2017). Driven by heightened cortical plasticity, the synaptic connections of binocular cells are reshaped and rewired under the influence of visual experience (Hooks and Chen, 2020). In this process, abnormal visual experience caused by imbalanced binocular input could lead to functional defects such as amblyopia (Holmes and Clarke, 2006). Interestingly, it has been reported that the variability of cortical responses is abnormally high in amblyopic monkeys (Wang et al., 2017), and juvenile dark rearing can reduce the reliability of V1 responses to natural scene stimulation (Ko et al., 2014). These results suggest that the maturation of variability and reliability may be driven by the developmental process of binocular vision and might be modulated by the critical period plasticity in V1.

Thus, it is important to know whether the binocular integration of variability and reliability in V1b malfunctions in amblyopic subjects and whether this defect can be rescued. To answer this question, we used *in vivo* extracellular electrophysiology to record neuronal responses with binocular, ipsilateral, or contralateral visual input. We addressed the following questions: (1) how variability and reliability are driven by the development of binocular vision, (2) whether critical period can regulate the variability and reliability of V1b neurons, and (3) how variability and reliability change with abnormal visual experience during development and whether they can be rescued. These investigations will enrich our understanding of the visual encoding characteristics and the functional connectivity for the formation of normal binocular vision.

RESULTS

Binocular input optimized the response variability and reliability in V1b neurons

To investigate the influence of binocular input on cortical response variability and reliability, we firstly recorded binocular, ipsilateral, and contralateral responses of V1b neurons (including both binocular and monocular cells) and contralateral response in V1m (only monocular cells), evoked by sinusoidal drifting grating stimuli (Video S1) with 8 different orientations in adult (P60) mice (Figures 1A–1C). For responses to repeated stimulation in the preferred orientation, Fano factors (FFs) and reliability indexes (RIs) were calculated to characterize the response variability for spike rates and the reliability for spike timing, respectively (see STAR Methods for details). Of all cortical neurons, which can respond significantly to any of the stimulus input (including binocular, ipsilateral, and contralateral input), the FFs of binocular response were the lowest among the four recording conditions (Figure 1D). Meanwhile, responses to binocular input are the most reliable (Figure 1E), indicating that binocular responses across the visual cortex have the optimal encoding fidelity (the lowest variability and the highest reliability). For the monocular response in V1b, contralateral response was less variable and more reliable than ipsilateral response. Comparing the contralateral response in V1b and V1m, the encoding fidelity of V1b was superior to V1m (Figures 1D and 1E). Furthermore, for binocular neurons with significant binocular, ipsilateral, and contralateral responses, the distribution of response variability and reliability with different visual input was similar to the overall results (Figures 1F and 1G), and the mean binocular FFs and RIs of binocular neurons in individual animals were also the optimal (Figures S1A and S1B). To examine if sex difference was involved in the response fidelity, we compared the variability and reliability between male and female mice and found there was no statistically significant difference except for the ipsilateral response (Figures S1C and S1D). Considering the numbers of female mice (N = 2) were much fewer than male (N = 13), and the maturation timeline for males and females were different, we thus excluded the female data from the analysis and our results were unaffected (Figures S1E–S1H). Therefore, we only include males in the following experiments and statistics. The results for female will be conducted in a following study. To explore the layer-specific distribution, we classified the cellular activities into superficial-middle layer (depth <500 μm) and deep layer (depth ≥500 μm) according to the depth of the recorded cells in V1b (Figure S2A) and did not find significant correlations between cellular depth and variability and reliability (Figures S2B and S2C), and the distribution of FFs and RIs for binocular neurons was also similar between superficial-middle layers and deep layers, although there was no significant difference for the distribution of FFs in deep layers between groups from different visual inputs (Figures S2D–S2G). In addition, we also assessed the correlation between FFs and RIs and found that FFs and RIs showed a stronger negative correlation in V1b than V1m (Figures 1H–1K), suggesting that increased response reliability was accompanied by decreased variability in V1b. Similar to grating stimulation, binocular reliability for animated movie stimulation was the highest among all recording conditions (Figures S3A, S3D, and S3E), and this movie stimuli, which contains specific gabor features compared with grating, showing higher complexity (Figures S3B, S3C, Video S2), can improve the response reliability for binocular responses (Figures S3D and S3E), consistent with previous studies (Rikhye and Sur, 2015; de Vries et al., 2020).
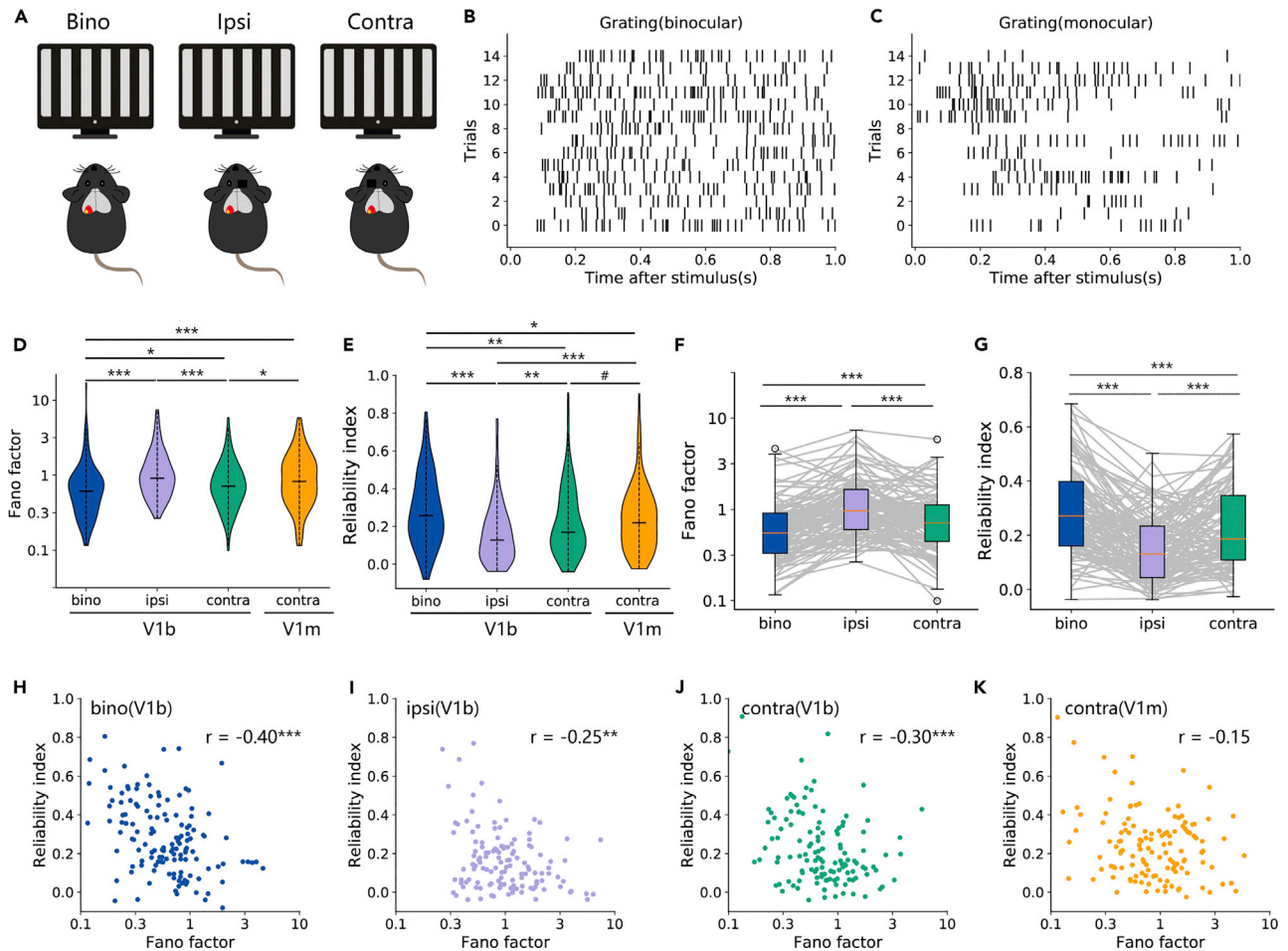
Figure 1. Response variability and reliability in V1b and V1m of adult mice

(A) Schematic diagram of binocular response, ipsilateral response, and contralateral response for V1 neurons when presenting grating stimulus.

(B–C) Raster plots of the firing pattern from different visual inputs (left: binocular input, right: monocular input) of V1b neuron with repeated grating stimulation (15 repeats).

(D) Distribution of Fano factors in the overall neuronal responses in different visual inputs (V1b: N = 15; V1m: N = 9,"N" indicates the numbers of mice). y axis represents the Log10 value of each Fano factor (same as below). From left to right represents the binocular response (bino, cells = 136, blue), ipsilateral response (ipsi, cells = 130, purple), contralateral responses (contra, cells = 130, green) in V1b, and contralateral responses (contra, cells = 130, yellow) in V1m. The medians of each group are 0.62, 0.91, 0.71, and 0.83. Statistical difference between two groups was assessed by Mann–Whitney U test: bino versus ipsi: $p = 1.37 \times 10^{-7}$***; bino versus V1b contra: p = 0.045*, bino versus V1m contra: p = 0.00051***. V1b contra versus ipsi: p = 0.00071***, V1b contra versus V1m contra: p = 0.048* (*p < 0.05; **p < 0.01; ***p < 0.001, # represents no significance).

(E) Distribution of reliability indexes in the overall neuronal responses in different visual inputs (V1b: N = 15; V1m: N = 9). From left to right represents the reliability index of binocular response (bino, cells = 136, blue), ipsilateral response (ipsi, cells = 130, purple), contralateral responses (contra, cells = 130, green) in V1b, and contralateral responses (contra, cells = 130, yellow) in V1m. The medians of each group are 0.26, 0.13, 0.17, and 0.22. Statistical difference between two groups was assessed by Mann–Whitney U test: bino versus ipsi: $p = 1.65 \times 10^{-8}$***; bino versus V1b contra: 0.0038**; bino versus V1m contra: p = 0.048*; V1b contra versus ipsi: p = 0.0030**, V1m contra versus ipsi: $p = 3.15 \times 10^{-5}$***, V1b contra versus V1m contra: p = 0.31#, # represents no significance.

(F) Distribution of FFs of neuronal responses to drifting grating stimulation in three visual inputs for same neurons in V1b (N = 15, cells = 111). Results from the same neurons are connected by gray lines. The differences between groups are compared with Wilcoxon signed rank test. bino versus ipsi: $p = 1.30 \times 10^{-13}$***; bino versus contra: p = 0.00054***, contra versus ipsi: $p = 5.71 \times 10^{-6}$***.

(G) Distribution of reliability of neuronal responses to drifting grating stimulation in three visual inputs for the same neurons in V1b (N = 15, cells = 111). Results from the same neurons are connected by gray lines. The differences between groups are compared with Wilcoxon signed rank test. bino versus ipsi: $p = 3.96 \times 10^{-11}$***; bino versus contra: $p = 3.06 \times 10^{-5}$***, contra versus ipsi: $p = 4.25 \times 10^{-6}$***.

(H–K) Scatterplot of Pearson's correlation between Fano factor and reliability index for the different visual state in V1 of adult mice. From left to right represents the binocular ($r = -0.40$, $p = 1.73 \times 10^{-6}$***), ipsilateral ($r = -0.25$, p = 0.0036**), contralateral responses ($r = -0.30$, p = 0.00048***) in V1b, and contralateral responses in V1m ($r = -0.15$, p = 0.090#). The Pearson correlation coefficient (r) is indicated at the upper right corner, *p < 0.05; **p < 0.01; ***p < 0.001).

To investigate the mechanism underlying the lower variability and higher reliability of binocular response in adult V1b, we calculated the predicted binocular response by linearly superposing the contralateral and ipsilateral response for the preferred orientation and compared the correlations between predicted and actual binocular encoding (variability and reliability) (Figure S4A). There was a significant sublinear correlation between the predicted and actual binocular responses (Figure S4C), consistent with a previous study (Zhao et al., 2013). Interestingly, the actual and predicted FFs were also sub-linearly correlated ($r = 0.76$), accompanied with a sublinear correlation between binocular and monocular FFs (Figures S4B and S4D–S4F), whereas the actual and predicted RIs were linearly correlated ($r = 0.71$), accompanied with a linear correlation between binocular and monocular RIs (Figures S4B and S4G–S4I). These results suggested that the binocular variability and reliability can be reasonably interpreted by the coordinated integration from two eyes in adult mice.

Considering the binocular neurons have ocular-specific receptive field offset in location and profile difference (Goncalves and Welchman, 2017), we wonder whether the difference in visual encoding between V1b and V1m could be due to different receptive field properties. Thus, we estimated the relationship between FFs, RIs, and properties of receptive field, and no significant correlation was found between FFs, RIs, and the RF azimuth, elevation, area of binocular, contralateral and ipsilateral responses in V1b, and contralateral response in V1m (Figures S5A–S5C and S6A–S6C). Furthermore, neither orientation selectivity (gOSI) nor preferred orientation can affect the FFs and RIs (Figures S5D, S5E, S6D, and S6E). FFs were also independent of changes in firing rates and no correlation between RIs and firing rates was found in adult mice (Figures S7A–S7D). Therefore, the possibility that receptive field, feature selectivity, and firing rate affected variability and reliability was very limited. In addition, we wonder whether the better encoding fidelity of binocular response can be explained by the enhancement of brightness and contrast of the visual stimuli perceived by two eyes. Thus, we evaluated the FFs and RIs of V1b neuronal response to stimuli with different brightness and contrast (100%, 50%, 25%), and found that neither brightness nor contrast can significantly change the variability and reliability of V1b (Figures S8A–S8L).

In addition, it is unknown whether different classes of neurons play distinct roles in response variability and reliability. To test this, we classified the neurons recorded in V1 into narrow-spiking and broad-spiking cells according to the spike waveform duration (Figures S9A and S9B) (see STAR Methods for details). The inter-spike intervals (ISIs) of narrow and broad-spiking units exhibited different distributions, as the ISIs for narrow-spiking units showed more concentrated distribution at shorter intervals compared with broad-spiking units (Figure S9C). Because the parvalbumin-expressing fast-spiking GABAergic interneurons have short-duration action potentials, whereas excitatory normal-spiking pyramidal neurons have long-duration action potentials, it is commonly accepted that the narrow-spiking units are putative inhibitory interneurons, and the broad-spiking units are putative excitatory neurons (Connors and Gutnick, 1990; Kawaguchi, 1993; Nowak et al., 2003; Niell and Stryker, 2008). In our study, the percentage of narrow-spiking cell was significantly lower than broad cell (narrow:11.7%, broad:89.3%). Comparing the binocular, ipsilateral, and contralateral FFs and RIs between the narrow and broad-spiking cells, we found that regardless of narrow or broad neurons, binocular responses showed the optimal encoding fidelity compared with monocular responses. Contralateral responses had higher reliability and lower variability than ipsilateral responses, which is similar to all neuronal responses in V1b (Figures S9D–S9G). In addition, the FFs and RIs of binocular and ipsilateral responses of narrow cells were similar to broad cells. For contralateral responses, the FFs of narrow cells were higher than broad cells, whereas the RIs of narrow and broad cells showed no difference (Figures S9H–S9M). Our results demonstrated that the response variability and reliability showed similar pattern in different cell types, indicating that the visual information encoding adopts a common strategy.

Response variability and reliability were immature during the critical period

The experience-dependent cortical plasticity during the critical period is required for the maturation of neural connections and visual functions (Gordon and Stryker, 1996). To answer how the response variability and reliability developed, FFs and RIs were measured in juvenile mice (P28-P30, at the peak of critical period plasticity). Similar to adults, binocular responses were more reliable than monocular responses in juvenile visual cortex (Figures 2A and 2B) and binocular neurons in V1b (Figures 2C and 2D). However, the binocular and contralateral FFs were more similar than RIs, indicating the development of binocular variability might be more significant. For individual animals, the distribution of mean values of binocular, ipsilateral, and contralateral FFs for binocular neurons also showed the similar results (Figures S1I and S1J). To better appreciate the developmental differences, cumulative distribution of FFs and RIs of V1b
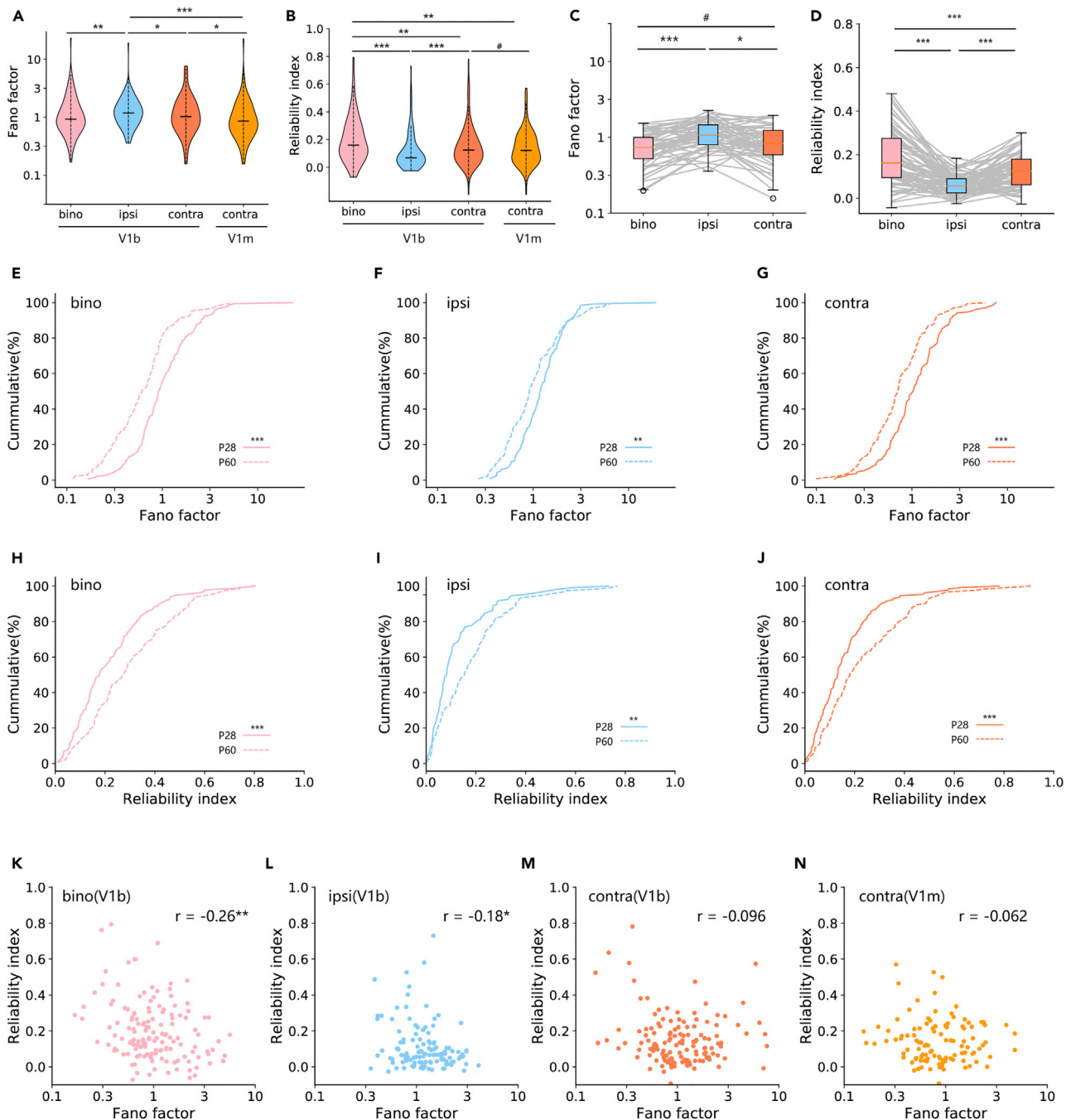
Figure 2. Response variability and reliability in V1b and V1m in juvenile mice

(A) Distribution of Fano factors in the overall neuronal responses of different visual inputs in juvenile (P28) mice (V1b: N = 9; V1m: N = 6, all males). From left to right, binocular response (bino, cells = 144, pink), ipsilateral response (ipsi, cells = 119, light-blue), contralateral responses (contra, cells = 136, orange) in V1b, and contralateral responses (contra, cells = 110, yellow) in V1m.The medians of each group are 0.92, 1.19, 1.03, and 0.86. Statistical difference between two groups was assessed by Mann–Whitney U test: bino versus ipsi: p = 0.0043**; bino versus V1b contra: p = 0.23#; bino versus V1m contra: p = 0.058#; V1b contra versus ipsi: p = 0.040*, V1b contra versus V1m contra: p = 0.014*.

(B) Distribution of reliability indexes in the overall neuronal responses of different visual inputs in juvenile mice (V1b: N = 9; V1m: N = 6). From left to right, binocular response (bino, cells = 144, pink), ipsilateral response (ipsi, cells = 119, light-blue), contralateral responses (contra, cells = 136, orange) in V1b, and contralateral responses (contra, cells = 110, yellow) in V1m.The medians of each group are 0.16, 0.069, 0.12, and 0.12. Statistical difference between two groups was assessed by Mann–Whitney U test: bino versus ipsi: p = 3.71 × 10^{-8}***; bino versus V1b contra: p = 0.0040**; bino versus V1m contra: p = 0.0026**; V1b contra versus ipsi: p = 0.0015**; V1b contra versus V1m contra: p = 0.79#.

Figure 2. *Continued*

(C) Distribution of Fano factor of neuronal responses to drifting grating stimulation in three visual inputs for same neurons in V1b (N = 9, cells = 174). Results from the same neurons are connected by gray lines. The differences between groups are compared with Wilcoxon signed rank test, bino versus ipsi: p = $7.57 \times 10^{-5***}$; bino versus contra: p = 0.23[#]; contra versus ipsi: p = 0.016*.

(D) Distribution of reliability index of neuronal responses to drifting grating stimulation in three visual inputs for same neurons in V1b (N = 9, cells = 174). Results from the same neurons are connected by gray lines. The differences between groups are compared with Wilcoxon signed rank test, bino versus ipsi: p = 1.04e-10***; bino versus contra: p = 0.00033***; contra versus ipsi: p = 0.00011***.

(E–G) Cumulative distributions of binocular, ipsilateral, contralateral FFs for binocular neurons in P28 and P60 V1b. From left to right, bino: p = $4.01 \times 10^{-8***}$, ipsi: p = 0.0047**, contra: p = $1.74 \times 10^{-5***}$.

(H–I) Cumulative distributions of binocular, ipsilateral, contralateral RIs for binocular neurons in P28 and P60 V1b. From left to right, bino: p = $9.98 \times 10^{-5***}$, ipsi: p = 0.0060**, contra: p = 0.00065***.

(K–N) Scatterplot of Pearson's correlation between Fano factor and reliability index for the different visual state in V1 of juvenile mice. From left to right represents the binocular (r = −0.26, p = 0.0015**), ipsilateral (r = −0.18, p = 0.046*), contralateral responses (r = −0.096, p = 0.27[#]) in V1b, and contralateral responses in V1m (r = −0.062, p = 0.52[#]). The Pearson correlation coefficient (r) is indicated at the upper right corner.

was compared between the juvenile and adult mice, showing that the encoding fidelity in juveniles was significantly immature compared with adults (Figures 2E–2J). Furthermore, in contrast to adults, the degree of negative correlation between FFs and RIs was reduced but still significant in juveniles, especially for the binocular responses (Figures 2K–2N). Similarly, the maturation of response reliability over development was also seen with movie stimulation (Figures S3E and S3G–S3J). Together, our results showed that the response variability and reliability was in an immature stage during the critical period, and the encoding fidelity was gradually improved with the maturation of binocular vision.

Disrupted binocular variability and reliability in amblyopic mice

V1b is a critical center for the establishment of binocular circuit, which is most severely affected by amblyopia (Kiorpes, 2006). We wonder whether neuronal response reliability and variability are affected in the abnormal binocular visual circuit in amblyopic mice. To approach this question, we performed long-term monocular deprivation (LTMD) from the onset of critical period (P21) to adulthood (P60) (Figure 3A), which is a well-studied animal model for amblyopia. As expected, LTMD induced robust ocular dominance shift with decreased contralateral bias index (Figures 3B and 3C), indicating the developmental dysfunction in the deprived eye. LTMD disrupted the encoding fidelity compared with control mice, with elevated FFs and decreased RIs of binocular and deprived-eye responses (Figures 3D and 3E). For non-deprived eye (ipsi), the reliability was enhanced while the variability remained unaffected. In individual animals, compared with controls, the FFs and RIs for binocular neurons in LTMD mice showed similarity among different visual inputs (Figures S1A, S1B, S1K, and S1L), underlying the disrupted binocular encoding fidelity. Interestingly, in control mice, the binocular FFs (bFF) have stronger correlation with ipsilateral FFs (iFF) than contralateral FFs (cFF), whereas the binocular RI (bRI) was more correlated with contralateral RI (cRI) (Figures 3F and S4B), which can be explained by the higher variability in ipsilateral response, whereas higher reliability in contralateral response, underlying that the binocular variability might be mainly contributed from ipsilateral input while binocular reliability was principally contributed from contralateral input. Strikingly, LTMD significantly disrupted the correlation of binocular and monocular FFs for binocular neurons. In addition, the reliability correlation between deprived (cRI) and binocular (bRI) input was also significantly disrupted, whereas the correlation for non-deprived (iRI) input remained unaffected (Figure 3F). Together, LTMD increased binocular variability and decreased binocular reliability, suggesting that the development of binocular variability and reliability is dependent on visual experience.

Reactivating cortical plasticity partially rescued the defects of response variability and reliability in amblyopic mice

It was reported that 10 days dark rearing (DR) could reactivate a persistent, juvenile-like ocular dominance plasticity in adults (Erchova et al., 2017), which enabled the rewiring of the visual circuit and contributed to the recovery of visual functions in amblyopic animals. To further explore whether the effect of abnormal visual experience on response variability and reliability can be reversed, we first assessed whether 10d DR can reactivate the ocular dominance plasticity in adults. 3d MD was performed following 10d DR of normal reared adult mice (Figure S10A). We observed a significant ocular dominance shift, as described in previous studies (Figure S10B) (Erchova et al., 2017). Meanwhile, the variability of deprived eye was increased and the reliability was decreased as expected (Figures S10C and S10D). Next, 10d DR, which can reopen a new critical period in adult V1b, were performed in LTMD mice, followed by 3d normal rearing (NR) (Figure 4A), which could enable the re-establishment of contralateral bias (Figure 4B). We analyzed the variability in the DR+3dNR mice and found that binocular FFs
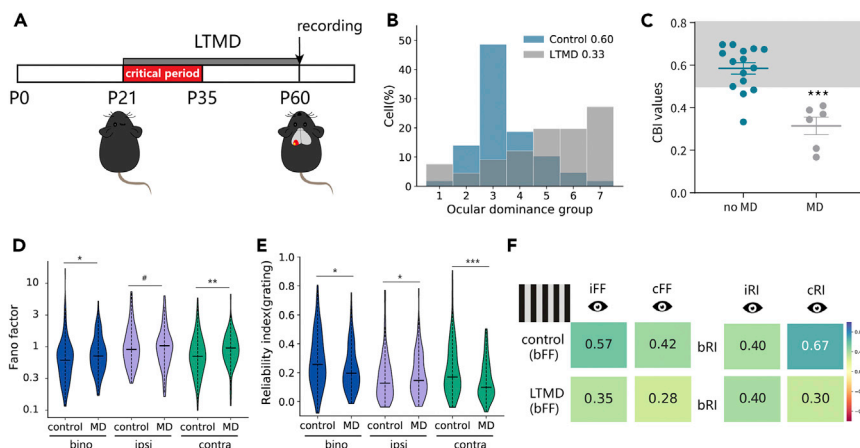
Figure 3. Effects of LTMD on response variability and reliability of V1b neurons

(A) Schematic diagram of monocular deprivation from critical period to adulthood.

(B) Distribution of ocular dominance group of between control and LTMD mice. Control group (N = 15, cells = 107), LTMD group (N = 6, all males, cells = 66); the CBI value of each group is represented by the number in the upper right corner.

(C) The graph shows the contralateral bias index (CBI) value for each mouse and the mean ± SEM for each group, each dot symbolizing the value from 1 mouse, p = 0.0002***, unpaired t test.

(D) Distribution of Fano factor for responses of V1b in control and LTMD adult mice. Control: mice = 15, cells = (bino:136, ipsi:130, contra:130); LTMD: N = 6, cells = (bino:91, ipsi:99, contra:83). The significance between LTMD and control: bino versus bino: p = 0.021*; ipsi versus ipsi: p = 0.49#; contra versus contra: p = 0.0037**, Mann-Whitney U-test.

(E) Distribution of reliability index (grating) for responses of V1b in control and LTMD adult mice. Control: mice = 15, cells = (bino:136, ipsi:130, contra:130); LTMD: N = 6, cells = (bino:91, ipsi:99, contra:83). The significance between LTMD and control: bino versus bino: p = 0.014*; ipsi versus ipsi: p = 0.048*; contra versus contra: p = 0.00082***, Mann-Whitney U-test.

(F) Pearson's correlations between binocular FFs, RIs, and monocular FFs, RIs in control and LTMD mice; color scale represents degree of correlation (blue positive; red negative); the significance of the correlations between different groups was tested: control: $r_{bFF\&iFF}$ versus $r_{bFF\&cFF}$ (z = 1.7701, p = 0.0384*, Pearson and Filon's z test); $r_{bRI\&iRI}$ versus $r_{bRI\&\ cRI}$ (z = −3.3570, p = 0.0004***, Pearson and Filon's z test); LTMD: $r_{bFF\&iFF}$ versus $r_{bFF\&cFF}$ (z = 0.8691, p = 0.1924, Pearson and Filon's z test); $r_{bRI\&iRI}$ versus $r_{bRI\&cRI}$ (z = 0.6610, p = 0.2543, Pearson and Filon's z test). Control versus LTMD: $r_{bFF\&iFF}$ versus $r_{bFF\&iFF}$ (z = 1.7882, p = 0.0369*, Fisher's z test); $r_{bFF\&cFF}$ versus $r_{bFF\&cFF}$ (z = 1.0143, p = 0.1552#, Fisher's z test); $r_{bRI\&iRI}$ versus $r_{bRI\&iRI}$ (z = 0.00003, p = 0.5000, Fisher's z test); $r_{bRI\&cRI}$ versus $r_{bRI\&cRI}$ (z = 3.1774, p = 0.0007***, Fisher's z test).

were even higher than LTMD mice, whereas ipsilateral FFs were increased and contralateral FFs were unchanged (Figure 4C), indicating that the binocular variability was not rescued by the reactivated cortical plasticity. Interestingly, our results revealed an enhanced reliability of deprived input and a decreased reliability in the non-deprived input in DR+3dNR mice (Figure 4D), demonstrating the reliability was rescued by the reactivated cortical plasticity. For individual animals, the distribution of FFs and RIs responding to different visual inputs was similar to normal adult mice although there was no significant difference among groups (Figures S1A, S1B, S1M, and S1N). Next, we analyzed the correlations between binocular and monocular FFs and RIs. Strikingly, in the DR+3dNR mice, the binocular variability and reliability correlation preference were restored, showing a high correlation between binocular and monocular FFs, similar to the control group, and the defected correlation between bRI and cRI was rescued (Figure 4E). In summary, plasticity that is reactivated by dark exposure can partially promote the recovery of response variability and reliability in the amblyopic visual cortex, suggesting the experience-dependent variability and reliability can be regulated by cortical plasticity (Figure 4F).

DISCUSSION

In this study, we investigated the effect of binocular vision on cortical response variability and reliability and found that the binocular response showed optimal visual encoding compared with the monocular response. Binocular inputs enabled the effective and reliable binocular responses in adults, whereas in juveniles, the binocular variability and reliability was immature. In amblyopic mice, the binocular variability and reliability were underdeveloped, accompanied with increased cortical variability and reduced reliability, and this defect can be partially restored by normal visual experience during the reactivated critical period, indicating that the response variability and reliability of visual cortex were dependent on visual experience, and the critical period plasticity was essential for the normal development of variability and
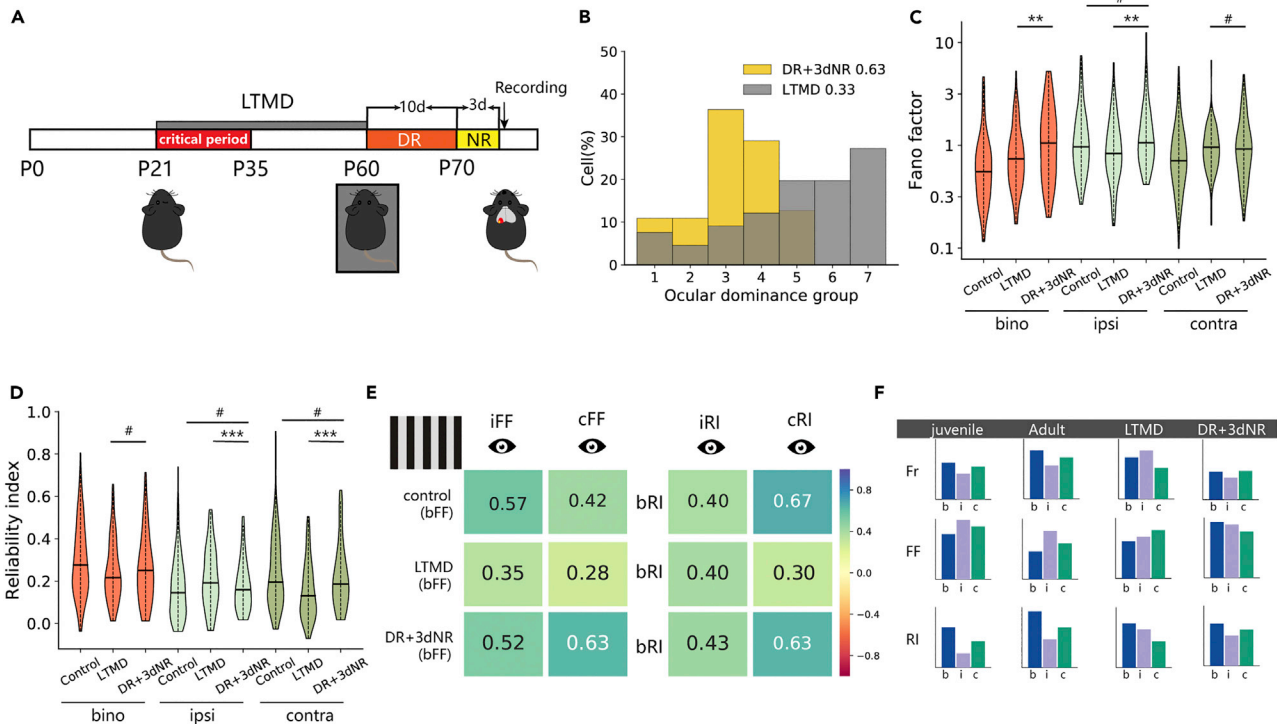
Figure 4. 10d dark rearing partially rescued variability and reliability in adult LTMD mice

(A) Schematic diagram of DR + NR in adult LTMD mice.

(B) 3d NR following 10d DR can restore ocular dominance in LTMD mice. LTMD group (mice = 6, cells = 66); DR+3dNR (mice = 4, cells = 52). The numbers in the figure indicate the CBI value.

(C) The distribution of Fano factor for grating stimulation in V1b of control, LTMD, and10dDR+3dNR mice. bino (LTMD, orange) versus bino (DR+3dMD, orange): p = 0.0047**; ipsi (LTMD, light green) versus ipsi (DR+3dMD, light green): p = 0.0063**; ipsi (DR+3dMD, light green) versus ipsi (control, light green), p = 0.15#; contra (LTMD, dark green) versus contra (DR+3dMD, light green): p = 0.42#, Mann–Whitney U test.

(D) The distribution of reliability index for grating stimulation in V1b of control, LTMD, and10dDR+3dNR mice. bino (LTMD, orange) versus bino (DR+3dMD, orange): p = 0.41#; ipsi (LTMD, light green) versus ipsi (DR+3dMD, light green): p = 0.00085***; ipsi (DR+3dMD, light green) versus ipsi (control, light green), p = 0.16#; contra (LTMD, orange) versus contra (DR+3dMD, light green), p = 0.00087***; contra (control, orange) versus contra (DR+3dMD, light green), p = 0.31#, Mann–Whitney U test.

(E) Pearson's correlations between binocular FFs, RIs, and monocular FFs, RIs in MD and DR+3dMD mice; color scale represents degree of correlation (blue positive; red negative). For the comparison of bFF(bRI) and iFF(iRI), cFF (cRI) in LTMD+3dNR: $r_{bFF\&iFF}$ versus $r_{bFF\&cFF}$ ($z = -0.9418$, p = 0.1732, Pearson and Filon's z test); $r_{bRI\&iRI}$ versus $r_{bRI\&cRI}$ ($z = -1.6226$, p = 0.0523, Pearson and Filon's z test). For the comparison of bFF(bRI), iFF(iRI), and cFF(cRI) between LTMD and LTMD+3dNR: $r_{bFF\&iFF}$ versus $r_{bFF\&iFF}$ ($z = -1.1174$, p = 0.1319, Fisher's z test); $r_{bFF\&cFF}$ versus $r_{bFF\&cFF}$ ($z = -2.4039$, p = 0.0081**, Fisher's z test); $r_{bRI\&iRI}$ versus $r_{bRI\&iRI}$ ($z = -0.1920$, p = 0.4239, Fisher's z test); $r_{bRI\&cRI}$ versus $r_{bRI\&cRI}$ ($z = -2.2882$, p = 0.0111*, Fisher's z test).

(F) The summary for the development of binocular variability and reliability in juvenile, NR, MD, DR+3dNR mice. Fr (firing rates), FF (Fano factor), RI (reliability index); each bar in the histogram represents the mean value of each group.

reliability (Figure 4F). Our results indicated that the maturation of binocular variability and reliability required gradual integration of the responses from two eyes during the development.

Binocular inputs enhanced encoding fidelity by elevating coherent connection strength of the network

Neuronal response variability and reliability, which is important for visual encoding, has been extensively studied in the mammalian visual system (Kara et al., 2000; Movshon, 2000). Several results have revealed that response variability arises from synaptic connections and is dependent on synaptic input, rather than from intrinsic properties of neurons (Markov et al., 2014; Lin et al., 2015). We found binocular neurons receiving synaptic inputs from two eyes showed reduced variability compared with monocular responses, which is consistent with a previous study reporting that the responses of neurons receiving higher contrast visual inputs showed reduced variability and increased reliability (Gómez-Laberge et al., 2016). In addition, variability of trial-averaged responses in visual cortex can be explained by the stabilized supra-linear network (SSN) model. Increased input of individual neurons enhances the supra-linear outputs that elevate

the gains of neurons and the effective synaptic strengths in the network (Ahmadian et al., 2013; Rubin et al., 2015). Stimulus-dependent changes in effective connectivity shape the magnitude and structure of activity fluctuations in the network. Therefore, an external stimulus can strongly modulate the variability of population activities (Hennequin et al., 2018). Binocular neurons receive coherent inputs from two eyes and produce more robust responses than neurons receiving monocular inputs, and the increased stimulus input can promote the ratio of inhibition to recurrent excitation received by neurons that facilitate variability quenching (Rubin et al., 2015). This conclusion is further substantiated by the results in our study that the response reliability of binocular neurons to complex stimuli (animated movie) is significantly improved compared with simple stimuli (drifting grating), which may be due to an enhancement of cortical inputs with complex stimulation, thus making the overall responses more reliable. Interestingly, the cooperative and homogeneous inputs of two eyes can be sub-linearly summated to predict the reliable binocular output, which may be critical for the establishment of binocular vision.

The reactivated plasticity partially rescued the response variability and reliability

Previous research has reported that binocular visual function such as ocular dominance, visual acuity, and binocular matching can be restored in amblyopic animals by dark rearing, which focused on reopening critical period plasticity in adulthood (He et al., 2007; Sale et al., 2007; Wang et al., 2010; Erchova et al., 2017). We assumed that the binocular variability and reliability can also be rescued by dark rearing. However, the changes of variability and reliability by DR followed by 3d normal visual experience do not fully match our expectations. Response variability and reliability can only be partially restored compared with LTMD mice (Figure 4F). Cortical variability and reliability are based on spike rates and timing, which can be affected by many factors, such as the awake state and cortical laminae. Considering the difference between Fano factor and reliability index, the absolute quantification for trial-to-trial variability can be affected more easily by these external changes (including the altered visual experience), compared with the relative quantification for reliability that may be more modulated by the developmental stages. Therefore, the DR-induced plasticity can more effectively rescue the response reliability, whereas variability can be greatly affected by the abnormal experience such as DR itself.

Limitations of the study

There are a few limitations in this study. Firstly, it should be noted that the results in our study were obtained from mice under anesthesia, which can induce higher cortical fluctuations and spontaneous activities compared with awake mice (Goltstein et al., 2015). Therefore, the overall cortical Fano factors we recorded might be overestimated than awake animals, according to the results that the variability in anesthetized animals was larger than awake accompanied with a higher noise correlation (Ecker et al., 2014). Secondly, we did not explore the detailed origin and specific mechanism of the decreased variability induced by binocular input. Thirdly, we only studied the cortical variability for single cell, ignoring the variability for population activity. In the last, the sex difference was not fully illustrated, which requires further investigation.

In summary, our study revealed the difference between variability and reliability in binocular and monocular responses, and its development following the maturation of binocular visual circuits. It is interesting to ask that along the visual pathway, how different brain regions contribute to the development of the visual encoding, considering the response variability is gradually enhanced from retina to LGN to V1 (Kara et al., 2000), and the circuit mechanisms regulating the variability and reliability remain to be investigated. Furthermore, how does the property of synaptic connectivity guide the animal's behavior through effective and reliable neuronal responses? All these problems are still worthy of in-depth exploration.

STAR★METHODS

Detailed methods are provided in the online version of this paper and include the following:

- KEY RESOURCES TABLE
- RESOURCE AVAILABILITY
  - Lead contact
  - Materials availability
  - Data and code availability
- EXPERIMENTAL MODEL AND SUBJECT DETAILS
  - Animals
- METHOD DETAILS
  - Monocular deprivation (MD)

- ○ *In vivo* electrophysiology
- ○ Visual stimuli
- ○ Sinusoidal patch
- ○ Drifting gratings
- ○ Animated movie
- QUANTIFICATION AND STATISTICAL ANALYSIS
  - ○ Spike sorting
  - ○ Quality control
  - ○ Receptive field
- GABOR FEATURE EXTRACTION
- CALCULATION OF MOVIE AND GRATING COMPLEXITY
- ORIENTATION SELECTIVITY
  - ○ Response variability and reliability
  - ○ Predicted binocular response and FF, RI
  - ○ Cell classification
  - ○ Other statistical analysis

SUPPLEMENTAL INFORMATION

Supplemental information can be found online at https://doi.org/10.1016/j.isci.2022.104984.

AUTHOR CONTRIBUTIONS

Conceptualization, Q.L. and Y.G.; Methodology, X.H. and Q.L.; Formal Analysis, X.H. and Q.L.; Investigation, X.H., Q.L., J.C. and N.L.; Writing—Original Draft, X.H. and Q.L.; Writing—Review & Editing, X.S. and Y.G.; Supervision, X.S. and Y.G.

DECLARATION OF INTERESTS

The authors declare no competing interests.

REFERENCES

Ahmadian, Y., Rubin, D.B., and Miller, K.D. (2013). Analysis of the stabilized supralinear network. Neural Comput. 25, 1994–2037.

Barthó, P., Hirase, H., Monconduit, L., Zugaro, M., Harris, K.D., and Buzsáki, G. (2004). Characterization of neocortical principal cells and interneurons by network interactions and extracellular features. J. Neurophysiol. 92, 600–608.

Borst, A., and Theunissen, F.E. (1999). Information theory and neural coding. Nat. Neurosci. 2, 947–957.

Churchland, M.M., Yu, B.M., Cunningham, J.P., Sugrue, L.P., Cohen, M.R., Corrado, G.S., Newsome, W.T., Clark, A.M., Hosseini, P., Scott, B.B., et al. (2010). Stimulus onset quenches neural variability: a widespread cortical phenomenon. Nat. Neurosci. 13, 369–378.

Cohen, M.R., and Maunsell, J.H.R. (2009). Attention improves performance primarily by reducing interneuronal correlations. Nat. Neurosci. 12, 1594–1600.

Connors, B.W., and Gutnick, M.J. (1990). Intrinsic firing patterns of diverse neocortical neurons. Trends Neurosci. 13, 99–104.

Contreras, D., and Palmer, L. (2003). Response to contrast of electrophysiologically defined cell classes in primary visual cortex. J. Neurosci. 23, 6936–6945.

de Vries, S.E.J., Lecoq, J.A., Buice, M.A., Groblewski, P.A., Ocker, G.K., Oliver, M., Feng, D., Cain, N., Ledochowitsch, P., Millman, D., et al. (2020). A large-scale standardized physiological survey reveals functional organization of the mouse visual cortex. Nat. Neurosci. 23, 138–151.

Diedenhofen, B., and Musch, J. (2015). cocor: a comprehensive solution for the statistical

comparison of correlations. PLoS One *10*, e0121945.

Ecker, A.S., Berens, P., Cotton, R.J., Subramaniyan, M., Denfield, G.H., Cadwell, C.R., Smirnakis, S.M., Bethge, M., and Tolias, A.S. (2014). State dependence of noise correlations in macaque primary visual cortex. Neuron *82*, 235–248.

Erchova, I., Vasalauskaite, A., Longo, V., and Sengpiel, F. (2017). Enhancement of visual cortex plasticity by dark exposure. Philos. Trans. R. Soc. Lond. B Biol. Sci. *372*, 20160159.

Faisal, A.A., Selen, L.P.J., and Wolpert, D.M. (2008). Noise in the nervous system. Nat. Rev. Neurosci. *9*, 292–303.

Garrett, D.D., Samanez-Larkin, G.R., MacDonald, S.W.S., Lindenberger, U., McIntosh, A.R., and Grady, C.L. (2013). Moment-to-moment brain signal variability: a next Frontier in human brain mapping? Neurosci. Biobehav. Rev. *37*, 610–624.

Ghanbari, A., Lee, C.M., Read, H.L., and Stevenson, I.H. (2019). Modeling stimulus-dependent variability improves decoding of population neural responses. J. Neural. Eng. *16*, 066018.

Goltstein, P.M., Montijn, J.S., and Pennartz, C.M.A. (2015). Effects of isoflurane anesthesia on ensemble patterns of Ca2+ activity in mouse v1: reduced direction selectivity independent of increased correlations in cellular activity. PLoS One *10*, e0118277.

Gómez-Laberge, C., Smolyanskaya, A., Nassi, J.J., Kreiman, G., and Born, R.T. (2016). Bottom-up and top-down input augment the variability of cortical neurons. Neuron *91*, 540–547.

Goncalves, N.R., and Welchman, A.E. (2017). "What not" detectors help the brain see in depth. Curr. Biol. *27*, 1403–1412.e8.

Gordon, J.A., and Stryker, M.P. (1996). Experience-dependent plasticity of binocular responses in the primary visual cortex of the mouse. J. Neurosci. *16*, 3274–3286.

Goris, R.L.T., Movshon, J.A., and Simoncelli, E.P. (2014). Partitioning neuronal variability. Nat. Neurosci. *17*, 858–865.

Gur, M., and Snodderly, D.M. (2006). High response reliability of neurons in primary visual cortex (V1) of alert, trained monkeys. Cereb. Cortex *16*, 888–895.

He, H.-Y., Ray, B., Dennis, K., and Quinlan, E.M. (2007). Experience-dependent recovery of vision following chronic deprivation amblyopia. Nat. Neurosci. *10*, 1134–1136.

Hennequin, G., Ahmadian, Y., Rubin, D.B., Lengyel, M., and Miller, K.D. (2018). The dynamical regime of sensory cortex: stable dynamics around a single stimulus-tuned attractor account for patterns of noise variability. Neuron *98*, 846–860.e5.

Holmes, J.M., and Clarke, M.P. (2006). Amblyopia. Lancet *367*, 1343–1351.

Hooks, B.M., and Chen, C. (2020). Circuitry underlying experience-dependent plasticity in the mouse visual system. Neuron *107*, 986–987.

Hubel, D.H., and Wiesel, T.N. (1962). Receptive fields, binocular interaction and functional architecture in the cat's visual cortex. J. Physiol. *160*, 106–154.

Hussar, C.R., and Pasternak, T. (2009). Flexibility of sensory representations in prefrontal cortex depends on cell type. Neuron *64*, 730–743.

Jacobs, E.A.K., Steinmetz, N.A., Peters, A.J., Carandini, M., and Harris, K.D. (2020). Cortical state fluctuations during sensory decision making. Curr. Biol. *30*, 4944–4955.e7.

Kara, P., Reinagel, P., and Reid, R.C. (2000). Low response variability in simultaneously recorded retinal, thalamic, and cortical neurons. Neuron *27*, 635–646.

Kawaguchi, Y. (1993). Groupings of nonpyramidal and pyramidal cells with specific physiological and morphological characteristics in rat frontal cortex. J. Neurophysiol. *69*, 416–431.

Kiorpes, L. (2006). Visual processing in amblyopia: animal studies. Strabismus *14*, 3–10.

Ko, H., Mrsic-Flogel, T.D., and Hofer, S.B. (2014). Emergence of feature-specific connectivity in cortical microcircuits in the absence of visual experience. J. Neurosci. *34*, 9812–9816.

Lin, I.C., Okun, M., Carandini, M., and Harris, K.D. (2015). The nature of shared cortical variability. Neuron *87*, 644–656.

Litwin-Kumar, A., and Doiron, B. (2012). Slow dynamics and high variability in balanced cortical networks with clustered connections. Nat. Neurosci. *15*, 1498–1505.

Markov, N.T., Ercsey-Ravasz, M.M., Ribeiro Gomes, A.R., Lamy, C., Magrou, L., Vezoli, J., Misery, P., Falchier, A., Quilodran, R., Gariel, M.A., et al. (2014). A weighted and directed interareal connectivity matrix for macaque cerebral cortex. Cereb. Cortex *24*, 17–36.

Movshon, J.A. (2000). Reliability of neuronal responses. Neuron *27*, 412–414.

Neske, G.T., Nestvogel, D., Steffan, P.J., and McCormick, D.A. (2019). Distinct waking states for strong evoked responses in primary visual cortex and optimal visual detection performance. J. Neurosci. *39*, 10044–10059.

Niell, C.M., and Stryker, M.P. (2008). Highly selective receptive fields in mouse visual cortex. J. Neurosci. *28*, 7520–7536.

Nowak, L.G., Azouz, R., Sanchez-Vives, M.V., Gray, C.M., and McCormick, D.A. (2003). Electrophysiological classes of cat primary visual cortical neurons in vivo as revealed by

quantitative analyses. J. Neurophysiol. *89*, 1541–1566.

Rikhye, R.V., and Sur, M. (2015). Spatial correlations in natural scenes modulate response reliability in mouse visual cortex. J. Neurosci. *35*, 14661–14680.

Rossi, L.F., Harris, K.D., and Carandini, M. (2020). Spatial connectivity matches direction selectivity in visual cortex. Nature *588*, 648–652.

Rubin, D.B., Van Hooser, S.D., and Miller, K.D. (2015). The stabilized supralinear network: a unifying circuit motif underlying multi-input integration in sensory cortex. Neuron *85*, 402–417.

Sale, A., Maya Vetencourt, J.F., Medini, P., Cenni, M.C., Baroncelli, L., De Pasquale, R., and Maffei, L. (2007). Environmental enrichment in adulthood promotes amblyopia recovery through a reduction of intracortical inhibition. Nat. Neurosci. *10*, 679–681.

Sarnaik, R., Wang, B.S., and Cang, J. (2014). Experience-dependent and independent binocular correspondence of receptive field subregions in mouse visual cortex. Cereb. Cortex *24*, 1658–1670.

Scholl, B., Pattadkal, J.J., and Priebe, N.J. (2017). Binocular disparity selectivity weakened after monocular deprivation in mouse V1. J. Neurosci. *37*, 6517–6526.

Shadlen, M.N., and Newsome, W.T. (1998). The variable discharge of cortical neurons: implications for connectivity, computation, and information coding. J. Neurosci. *18*, 3870–3896.

Vorobyov, V., Schwarzkopf, D.S., Mitchell, D.E., and Sengpiel, F. (2007). Monocular deprivation reduces reliability of visual cortical responses to binocular disparity stimuli. Eur. J. Neurosci. *26*, 3553–3563.

Wang, B.S., Sarnaik, R., and Cang, J. (2010). Critical period plasticity matches binocular orientation preference in the visual cortex. Neuron *65*, 246–256.

Wang, Y., Zhang, B., Tao, X., Wensveen, J.M., Smith, E.L., and Chino, Y.M. (2017). Noisy spiking in visual area V2 of amblyopic monkeys. J. Neurosci. *37*, 922–935.

Waschke, L., Kloosterman, N.A., Obleser, J., and Garrett, D.D. (2021). Behavior needs neural variability. Neuron *109*, 751–766.

White, B., Abbott, L.F., and Fiser, J. (2012). Suppression of cortical neural variability is stimulus- and state-dependent. J. Neurophysiol. *108*, 2383–2392.

Zhao, X., Liu, M., and Cang, J. (2013). Sublinear binocular integration preserves orientation selectivity in mouse visual cortex. Nat. Commun. *4*, 2088.

STAR★METHODS

KEY RESOURCES TABLE

REAGENT or RESOURCE	SOURCE	IDENTIFIER
Chemicals		
Urethane	Sigma-Aldrich	U2500; CAS:51-79-6
Chlorprothixene	Sigma-Aldrich	C1671; CAS:6469-93-8
Isoflurane	RWD	R510-22-8
Experimental models: Organisms/strains		
Mouse, C57BL/6J	Shanghai Shrek Experimental Animal Co., Ltd	N/A
Software and algorithms		
MATLAB	Mathworks	R2018b; http://www.mathworks.com
Python 3.7	Python Software Foundation	http://www.python.org
Plexon	Plexon	https://plexon.com

RESOURCE AVAILABILITY

Lead contact

Further information and requests for resources and reagents should be directed to and will be fulfilled by the lead contact, Dr. Yu Gu (guyu_@fudan.edu.cn).

Materials availability

This study did not generate new unique reagents.

Data and code availability

All data reported in this paper will be shared by the lead contact upon request.

This paper does not report original code.

Any additional information required to reanalyze the data reported in this paper is available from the lead contact upon request.

EXPERIMENTAL MODEL AND SUBJECT DETAILS

Animals

Wild-type C57BL/6J mice, mainly males (unless specifically stated) and aged between postnatal day(P)28-30, P60-P90, were used in the study, which were purchased from Shanghai Shrek Experimental Animal Co., Ltd. Mice were reared in a normal 12 h light/dark cycle, with food and water available *ad libitum*. For dark rearing mice, animals were raised in a small dark box with a black light-absorbing cloth. All procedures conform to the guidelines of Fudan University Experimental Animal Ethics Committee.

METHOD DETAILS

Monocular deprivation (MD)

Under the anesthesia of isoflurane (5% induction, $2 \pm 0.5\%$ maintenance), the upper and lower eyelids of the left eye were trimmed and then sutured together. Erythromycin ointment was applied daily for 7 days after operation to prevent infection and inflammation. At the same time, suture opening was checked daily. In this study, long-term MD (LTMD) was performed at postnatal day 21 (P21), and was reopened at P60 under the isoflurane anesthesia, by cutting tissue along the suture, and disqualified in the event of abnormal conditions such as turbidity in the eyeball.

In vivo electrophysiology

Mice were anesthetized with 10% urethane (1.25g/kg, i.p., Sigma), and further sedated with chlorprothixene (10 mg/kg, i.m., Sigma). Silicone oil was applied to the eye surface to prevent drying. Lincomycin and

Lidocaine Hydrochloride Gel was applied on the head skin. When the muscle strength of the mice disappeared, the scalp and soft tissue overlying the skull were incised to expose the skull surface. The binocular area (V1b) of the left V1 was marked 1.0 mm anterior to the sagittal suture and 3.0 mm lateral to the midline, and V1m located 2.0 mm lateral to the midline and 1.0 mm anterior to the sagittal suture. A stainless-steel ring was tightly glued to the skull with dental cement, and the head was fixed onto a customized stereotaxis through the ring, and additional oxygen with 0.4 atmospheric pressure was supplied. The body temperature was maintained at 37°C by a feedback heating pad (Harvard Apparatus). A 1 mm^2 window was drilled on the skull to expose the brain surface. Artificial cerebrospinal fluid (ACSF, containing 140 mM NaCl, 2.5 mM KCl, 11 mM Glucose, 20 mM HEPES, 2.5 mM CaCl$_2$, 3 mM MgSO$_4$, 1 mM NaH$_2$PO$_4$, pH 7.3-7.4, osmotic pressure adjusted to about 310 mOsmol) was applied on the brain surface to prevent tissue drying or hardening. The dura mater was removed with a slightly curved needle tip. The extracellular electrical activity of neurons was *in vivo* recorded by Plexon OmniPlex multichannel neural signal acquisition system, and the sampling frequency was 40 kHz. Multichannel silicon electrodes (Asy-1-16-1-6mm, Louts Biochips; A4x8-5mm-50-200-177, Neuronexus Technologies) were inserted into the brain with a micromanipulator. The tip of the electrode was usually 500-600 μm below the surface of the brain. The recording sites of the electrodes were spanning throughout different layers of the cortex. After electrode insertion, we usually waited about 30 min before recording to allow the brain tissue fully rebound to eliminate the activity suppression by tissue damage. After each experiment, eyeball was checked again to ensure the validity of the experimental data, and then the mouse was sacrificed.

Visual stimuli

Visual stimuli were generated by a customized script written in PsychoPy and played on Dell e1715s monitor (resolution 1280 × 1024, screen width 34 cm, refresh rate 60 Hz). The monitor was placed 20 cm in front of the mouse, and the center of the monitor was aligned to the center of the two eyes. The visual stimuli presented by the monitor occupied the visual field of 96 × 80°. During the experiment, response was recorded following the sequence of binocular, ipsilateral (left eye) and contralateral (right eye) input. For monocular response, the other eye was covered with a customized black opaque tape. The visual stimuli consist of three parts: sinusoidal patch, drifting gratings and animated movie. There is a 20 s dark period between the adjacent two parts.

Sinusoidal patch

The sinusoidal patch stimuli are composed of sinusoidal drifting gratings with spatial frequency of 0.04 cpd (cycle per degree), temporal frequency of 2 Hz, and contrast of 100%, filling a 16° diameter circular area. The rest of the screen remains gray with intermediate brightness. Each time, the sinusoidal patch would appear randomly at one of the 120 sites on the screen (the screen is divided by a grid of 12 × 10, and the distance between the two adjacent sites is 8°) and lasts for 250 ms. The plaque is continuously presented with no interval. For each site, the gratings consist of 0°, 45°, 90°,135°, 180°, 225°, 270 and 315° directions, respectively, and move perpendicular to that in one of two directions.

Drifting gratings

The drifting grating stimuli (see Video S1) are sinusoidal drifting gratings in full screen with spatial frequency of 0.04 cpd, temporal frequency of 2Hz and contrast of 100%. The gratings have eight different directions of 0°, 45°, 90°, 135°, 180°, 225°, 270 and 315°, and move perpendicular to that in one of two directions. Each stimulus lasts for 1.5 s, and there is a 1.5 s Gy screen (blank stimulus) between the two adjacent stimuli. Each stimulus repeated 15 times.

Animated movie

The animated movie (see Video S2) was selected from the 37-47 s of *Tom and Jerry: Puss gets the boot*, a total of 300 frames, which includes a lot of motion elements. The original movie was converted from color to gray, and its original resolution is 496 × 360 pixels. When the movie was actually played, it occupies a visual field of 96 × 80°, and the remaining edge of the screen remains gray. The movie is played at a refresh rate of 30 frames per second for 10 s and repeated 10 times, with a 2-s gray screen interval between adjacent repeats.

QUANTIFICATION AND STATISTICAL ANALYSIS

Data quantification and statistical analysis was conducted through customized scripts written in *Python*, using software packages mainly include *Numpy, SciPy, IPython, Pandas, Matplotlib, Jumper, PIL* and *scikit-learn*. KiloSort and Phy (https://github.com/cortex-lab/KiloSort) were used for single unit isolation.

Spike sorting

Spike sorting was performed using Kilosort2 that tracks drifting clusters to automatically cluster units from raw data (https://github.com/MouseLand/Kilosort2) followed by manual curation of the units using 'Phy'-gui to ensure single unit isolations. For the obvious noise units (including the spike waveform with no obvious peaks and troughs; the waveform between different recording sites does not vary linearly along the site distribution) was excluded from the subsequent analysis.

Quality control

To ensure the isolation quality of individual units, the following criteria was utilized:

Inter spike interval (ISI) violations

We calculated the fraction of inter spike interval (ISI) violations within a 2 ms refractory period, and single-units were included for further analysis only if their spike waveforms formed well-isolated clusters, whose inter-spike-interval (ISI) violations <0.1.

Amplitude Cutoff

Given the excessive high spike threshold may cause the spike missing, we calculated the distribution of spikes histogram and the truncated part of the amplitude distribution of spike potentials. The proportion of missing spike potentials can be qualified as Amplitude Cutoff, and the isolated units whose Amplitude Cutoff value <0.05 were included in the further analysis.

Receptive field

By calculating the firing rates of each neuron with the sinusoidal patch stimulation, a two-dimensional distribution histogram was constructed as the receptive field of the unit, which was presented as a 10 × 12 matrix. Independent *Chi* square test was used to confirm whether the responses in each of the stimulation position was significant. We calculated $\chi^2 = \sum_{i=0}^{n} \frac{(\overline{R} - R_i)^2}{\overline{R}}$, where $R_i = \frac{1}{m}\sum_{j=0}^{m} E_{i,j}$, is the mean firing rates of each unit corresponding to *m* times of stimulation at site *i* in the sinusoidal patch stimulation, $\overline{R} = \frac{1}{n}\sum_{i=0}^{n} R_i$, is the overall average of firing rates. The spike numbers and stimulating conditions were randomly combined and repeated 2000 times to obtain the null hypothesis for average spiking at each site and the null hypothesis for χ^2. The p value was calculated by comparing the χ^2 for receptive field to null hypothesis. When p < 0.05, it is considered that there is a significant response of the unit under the stimulating condition. Then the receptive field was expanded from 10 × 12 to 80 × 96, and smoothed by bicubic interpolation. 99% of the null hypothesis of the average firing rates at each site was selected as the threshold, and the size of the suprathreshold part taken as the size of the receptive field, and $X_r = \frac{\sum x_i * T_i}{\sum T_i}$, $Y_r = \frac{\sum y_i * T_i}{\sum T_i}$ were calculated as the azimuth and elevation center of the receptive field, where x_i, is the horizontal and vertical coordinates of the suprathreshold part of the smoothed receptive field, T_i is the response intensity corresponding to the point.

GABOR FEATURE EXTRACTION

A total of 1576 Gabor filters were used to extract the feature information of video stimuli. For each filter, a feature queue consisting of 300 eigenvalues was generated, and each eigenvalue corresponds to a frame.

Gabor filter is the product of sine function and two-dimensional Gaussian space density function. The real number part is expressed as:

$$G(x, y; x_0, y_0, \lambda, \theta, \psi, \sigma, \gamma) = e^{-\frac{(x'^2 + \gamma^2 y'^2)}{2\sigma^2}} \cos\left(2\pi \frac{x'}{\lambda}\right) + \varphi$$

where.

$$x' = (x - x_0) * \cos\theta + (y - y_0) * \sin\theta$$
$$y' = -(x - x_0) * \sin\theta + (y - y_0) * \cos\theta$$

x_0, y_0 is the center of the two-dimensional Gaussian space density function. In this experiment, the resolution of each frame was reduced to 192x160, corresponding to the size of 96x80. The whole space was divided by grids of 13x11, 7x6 and 3x2, corresponding to 16x16, 32x32 and 64x64 filters respectively. Each grid corresponds to the center of a Gabor filter, and there exists overlap between two adjacent Gabor filter sites. λ is the wavelength of the sine function, and its reciprocal is the spatial frequency of the sine function in the unit of visual field angle. In this experiment, the spatial frequency is 0.04 cpd, which is consistent with the grating stimulation, so λ is 25°.

θ is the direction of the sine function, and was set as 0°, 45°, 90° and 135°.

ψ represents the phase shift of the sine function, which was set to 0 and 90°.

σ reflects the dispersion degree of Gaussian space density function, which was set as $^1/_3$ of the filter size in this experiment.

γ is the aspect ratio of Gaussian space function, which was set to 1 in the experiment, suggesting that the shape of Gaussian space function is circular.

The formula to calculate eigenvalue is:

$$F = \sum G(x, y; x_0, y_0, \lambda, \theta, \psi, \sigma, \gamma) \cdot I_{plate}(x, y)$$

where $I_{plate}(x, y)$ is the grayscale array of the image corresponding to the filter position minus the average grayscale of the part on the image. When the center of the filter is located at the edge of the image, the center grayscale was used to fill the blank, which is consistent during the stimulation. The 300 eigenvalues of each filter were normalized.

CALCULATION OF MOVIE AND GRATING COMPLEXITY

The movie and video were decomposed into 300 image frames. For each frame, fast Fourier transform was used to reduces the frequencies of the image linearly and returns the sum of all pixels, the mean of summed pixels of 300 frames was regarded as the complexity.

ORIENTATION SELECTIVITY

One-way ANOVA was used to compare whether there were significant differences in the response of neurons between grating and blank stimulation. If the firing rates during the grating stimuli were significantly higher than blank stimuli ($p < 0.05$) for at least one orientation, the neuron was considered sensitive to that orientation. For the neurons sensitive to drifting grating stimulation, global orientation selective index (gOSI) was calculated as gOSI $= \frac{\sum R_\theta * e^{2*i\theta}}{\sum R_\theta}$, Where R_θ is the average firing rates of the grating moving at θ orientation, minus the average firing rates of blank stimulation.

Single sample t-test was used to compare whether there were significant differences in the response of neurons between the animated movie stimuli and the 20 s blank stimuli. If $p < 0.001$, the neuron was considered sensitive to the animated movie stimulation.

Response variability and reliability

In studies of visual system, spike variability is often quantified by the ratio of variance to mean spike count, defined as the Fano factor (FF)(Gur and Snodderly, 2006; Cohen and Maunsell, 2009; Ghanbari et al., 2019). FF has a value of 1 if responses are as variable as a Poisson process, in which individual action potentials are generated at random times according to a time-varying firing rate (Gur and Snodderly, 2006; Cohen and Maunsell, 2009; Ghanbari et al., 2019). For drifting grating stimulus at the preferred direction, response variability was measured by calculating $F = \frac{variance(R_\theta)}{Mean(R_\theta)}$ as the Fano factor, the ratio of the variance and the mean of firing rates with repeated stimulation. For a Poisson process with a fixed firing rate, the

Fano factor should be 1, so Fano factors above 1 may be interpreted as significant variability in a neuron's underlying firing rate (Litwin-Kumar and Doiron, 2012).

For the same visual stimuli, the response reliability can be represented as the average of the correlation coefficient of the time series of neuronal firing between repeated stimuli (Rikhye and Sur, 2015). For sinusoidal grating stimulation, we calculated reliability index for grating stimulation (gRI): $R_{pref\theta} = \frac{2}{T^2-T}\sum_{i=1}^{T}\sum_{j=i+1}^{T}\rho(f_{i,pref\theta}, f_{j,pref\theta})$, where T is the number of repetitions of gratings in the optimal direction, $f_{i,pref\theta}$ is the distribution histogram of the neuronal firing rates in the 1.5 s stimulating time in 100 ms bins, $\rho(f_{i,pref\theta}, f_{j,pref\theta})$ is the Pearson correlation coefficient. For animation movie stimulation, the same method was used to calculate reliability index for movie stimulation (mRI): $R_{movie} = \frac{2}{T^2-T}\sum_{i=1}^{T}\sum_{j=i+1}^{T}\rho(f_{i,movie}, f_{j,movie})$.

Predicted binocular response and FF, RI

For neurons with obvious response to sinusoidal grating stimulation in all three visual inputs, the evoked spikes of ipsilateral and contralateral inputs under the same optimal direction are linearly superimposed, and we calculated the predicted binocular Fano factor and reliability index.

Ocular dominance index (ODI) and contralateral bias index (CBI).

For neurons sensitive to sinusoidal grating stimulation in ipsilateral and contralateral responses, the ocular dominance index of each neuron was calculated (Hubel and Wiesel, 1962) as:

$$ODI = \frac{C-I}{C+I}$$

Where I and C are the difference between the response in the preferred direction and the spontaneous firing rates under the ipsilateral and contralateral vision, respectively.

According to ODI, neurons can be divided into 1-7 groups, - 1 to - 0.6 is Group 1, - 0.6 to - 0.4 is Group 2, - 0.4 to - 0.1 is Group 3, - 0.1 to 0.1 is Group 4, 0.1 to 0.4 is Group 5, 0.4 to 0.6 is Group 6, 0.6 to 1 is Group 7. Group 1 neurons are dominated by contralateral response, while Group 7 neurons are dominated by ipsilateral response.

The contralateral bias index is calculated as:

$$CBI = \frac{(n1-n7)+\frac{2}{3}(n2-n6)+\frac{1}{3}(n3-n5)+N}{2N}$$

Where N is the sum of the neuron number, and n1 to n7 are the number of neurons in the seven groups, respectively.

Cell classification

It has been well-established that inhibitory interneurons can be distinguished from pyramidal neurons by the shorter duration of their action potentials, less response adaptation, and higher firing rates (Connors and Gutnick, 1990; Contreras and Palmer, 2003; Barthó et al., 2004), so we classified our neurons on the basis of their waveform duration by measuring the time between the trough and the peak of action potentials and physiologically classified neurons into two distinct classes, narrow-spiking neurons (putative inhibitory interneuron) with spike durations of <500 μs and broad-spiking neurons (putative excitatory projecting pyramidal neurons) with spike durations of >500 μs (Hussar and Pasternak, 2009).

Other statistical analysis

No statistical methods were used to predetermine sample sizes, but our sample sizes are similar to those reported in the field (Gordon and Stryker, 1996; Cohen and Maunsell, 2009). All values were presented as mean ± SEM unless specifically stated. Mann-Whitney U test was the main statistic method used to compare the differences between groups, and differences of accumulative distribution between groups were tested for significance using the Kolmogorov-Smirnov (K-S) test.

Linear correlation between two variables was analyzed using the Pearson correlation coefficient (r). Throughout this work, 'correlation' denotes Pearson's correlation coefficient (Pearson's r). $0 \leq |r| \leq 0.20$ was considered as no or little correlation; $0.20 \leq |r| < 0.40$: weak (positive or negative) correlation; $0.40 \leq |r| \leq 0.60$: modest correlation; $0.60 \leq |r| \leq 0.80$: strong correlation; and $0.80 \leq |r| \leq 1$: very strong correlation. Other statistic methods used were specifically mentioned in the text. Noted that due to the distribution characteristics of Fano factor, the original value was used in the between-group comparison, while the logarithm with the original value of 10 as the base was used in the correlation analysis. The significance was expressed as follows: #: no significant difference, *: $p < 0.05$, **: $p < 0.01$, ***: $p < 0.001$.

The significance for the difference between two correlations based on dependent groups was conducted a Pearson and Filon's z test using the package cocor (Diedenhofen and Musch, 2015), for independent groups, correlation values were Fisher z -transformed to test the significance between different groups.